Acta Crystallographica Section D
Biological Crystallography
ISSN 0907-4449

Structures of the dimerization domains of the *Escherichia coli* disulfide-bond isomerase enzymes DsbC and DsbG

Shin-Mei Yeh, Nayden Koon, Christopher Squire and Peter Metcalf*

School of Biological Sciences, Auckland University, Auckland, New Zealand

Correspondence e-mail: peter.metcalf@auckland.ac.nz

Received 18 October 2006
Accepted 22 January 2007

PDB References: NDsbC, 2iyj, r2iyjsf; NDsbG, 2iy2, r2iy2sf.

DsbC and DsbG are periplasmic disulfide-bond isomerases, enzymes that facilitate the folding of secreted proteins with multiple disulfide bonds by catalyzing disulfide-bond rearrangement. Both enzymes also have *in vitro* chaperone activity. The crystal structures of these molecules are similar and both are V-shaped homodimeric modular structures. Each dimeric molecule contains two separate C-terminal thioredoxin-fold domains, joined by hinged helical 'stalks' to a single N-terminal dimerization domain formed from the N-terminal 67 residues of each monomer. In this work, the crystal structures of the separate DsbC and DsbG dimerization domains have been determined at resolutions of 2.0 and 1.9 Å, respectively. The two structures are both similar to the corresponding domains in the full-length molecules, showing that the dimerization domains fold independently of the catalytic portions of the full-length molecules. Localized structural differences between DsbC and DsbG were observed near the dimer interface and may be relevant to the different functions of the two enzymes.

1. Introduction

Disulfide-bond formation and isomerization play a significant role in protein folding and stability. The processes of disulfide-bond formation and isomerization are comparatively well understood for proteins secreted into the periplasm of Gram-negative bacteria. In *Escherichia coli*, the relevant *dsb* gene products fall into two separate electron-transport pathways: an oxidative pathway leading to the formation of substrate disulfide bonds and a reductive pathway leading to the breaking of substrate disulfide bonds, for example during disulfide-bond isomerization (Kadokura *et al.*, 2003). In the *Escherichia coli* oxidative pathway, DsbA, a 21 kDa monomeric member of the thioredoxin-fold superfamily, catalyses the formation of disulfide bonds in folding proteins, transferring its active-site disulfide bond to substrate. The DsbA disulfide active site is re-oxidized by DsbB, a 20 kDa transmembrane protein. In the reductive pathway, two homologous dimeric enzymes, DsbC and DsbG, catalyze the rearrangement of non-native disulfide bonds and DsbD, a transmembrane protein consisting of α, β and γ subunits, maintains the dithiol active sites of the two enzymes in the functional reduced state.

The atomic structures of oxidized and reduced DsbC from *E. coli* have been reported previously (McCarthy *et al.*, 2000; Banaszak *et al.*, 2004). The structures are similar and reveal a V-shaped homodimeric molecule, with each monomer comprised of a separate C-terminal thioredoxin-fold domain, joined by a hinged helical 'stalk' to a 67-residue N-terminal dimerization domain. The atomic structure of DsbG has also

been determined (Heras *et al.*, 2004). DsbG also shares the same basic V-shaped modular homodimeric structure as DsbC.

The DsbC dimerization domain is essential for isomerase activity, both *in vitro* and in the periplasm. Monomeric DsbC constructs generated by selective mutations in the DsbC dimer interface exist in the oxidized form *in vivo* and have no isomerase activity (Bader *et al.*, 2001). We have previously demonstrated that the DsbC dimerization domain is essential for the reduction of DsbC by DsbD (Goldstone *et al.*, 2001). Furthermore, the structure of the DsbC–DsbDα complex shows that the dimeric form of DsbC interacts with DsbDα *via* both catalytic domains (Goldstone *et al.*, 2001; Haebel *et al.*, 2002), providing a structural explanation for the requirement of the DsbC dimerization domain for the interaction with DsbD. Dimerization has also been reported to be essential for the *in vitro* chaperone activity of DsbC (Chen *et al.*, 1999). Although the structure and function of DsbC have been characterized and the functional role of the dimerization domain has been established, it has yet to be established if the DsbC dimerization domain folds independently from the rest of the DsbC molecule.

The biological function of DsbG has previously been characterized *in vivo* and has also been investigated using *in vitro* assays. DsbG is a homologue of DsbC, with 28% amino-acid sequence, and has a related biological function to that of DsbC (Andersen *et al.*, 1997; Bessette *et al.*, 1999). DsbG exhibits disulfide-isomerase activity with a narrower range of substrates than DsbC (Bessette *et al.*, 1999) and, like DsbC, maintains its active form *via* DsbD reduction (Andersen *et al.*, 1997). Futhermore, DsbG has chaperone activity *in vitro* (Shao *et al.*, 2000). Although the structure and function of full-length DsbG have been investigated, the importance of dimerization for the function of DsbG is not as well established as for that of DsbC.

In this investigation, we report the determination of crystal structures of the isolated dimerization domains of both DsbC (NDsbC) and DsbG (NDsbG) to resolutions of 2.0 and 1.9 Å, respectively. We describe the two truncated structures, comparing both the whole dimerization domains and the individual monomers with each other as well as with the corresponding domains and monomers from the full-length molecules. The overall structure of the dimerization domains and the corresponding domains from the full-length molecules are very similar, indicating that the domains fold independently. While the DsbC and DsbG dimerization domains are broadly similar, interesting differences were observed near the centre of the dimer interface that may be relevant to the different functions of the molecules in *E. coli*.

2. Materials and methods

2.1. Cloning

In the following PCR reactions and cloning, all primers and enzymes were supplied by Invitrogen, with the exception of *Nco*I and *Bam*HI, which were from Roche.

Table 1
Data-collection and refinement statistics.

	NDsbC	NDsbG
Space group	$P6_522$	$P4_1$
Unit-cell parameters (Å)	$a = b = 42.1$, $c = 268.7$	$a = b = 56.8$, $c = 42.0$
Resolution range (Å)	44.8–2.0 (2.07–2.0)	56.8–1.9 (2.0–1.9)
Unique reflections	10340 (847)	10806 (1564)
Data redundancy	12.9 (4.5)	3.4 (3.4)
Completeness (%)	97.2 (84.4)	99.4 (99.6)
$I/\sigma(I)$	36.6 (3.6)	9.3 (3.3)
Solvent content (%)	31.3	39.4
$R_{\rm merge}$ (%)	7.6 (54.4)	12.1 (30.6)
$R_{\rm work}$ (%)	0.227	0.195
$R_{\rm free}$ (%)	0.251	0.237
No. of residues	142	134
No. of waters	62	60
Residues in Ramachandran core region (%)	94.2	94.2
R.m.s.d. bond length (Å)	0.011	0.014
R.m.s.d. bond angle (°)	1.41	1.45
Average *B* factors (Å^2)	22.4	20.4

The gene encoding NDsbC (residues 1–71 of DsbC) was PCR-amplified from a subclone originating from DsbC-pET22b (Goldstone *et al.*, 2001) using the following primers containing restriction sites for the enzymes *Sal*I and *Pst*I: 5′-CAG GCG TCG ACC AGG CTG ATG AC-3′ and 5′-GGT GGT CTG CAG TCA CTA CAA CTG CTT TAA CAG CAT CTT ATT GG-3′. The gene encoding NDsbG (residues 1–71 of DsbG including an additional Cys at the C-terminus) was PCR-amplified from a subclone originating from pETdsbg (a gift from J. Bardwell; Shao *et al.*, 2000) using the following primers containing restriction sites for the enzymes *Nco*I and *Bam*HI: 5′-C TTC GCC ATG GAA CTT CCT GCT CC-3′ and 5′-G TCC GGC GGA TCC TTA ACA TTC TTT TTC G-3′. Both constructs lack the native signal sequence and the DsbG construct has a Glu1Met mutation resulting from the incorporation of the *Nco*I cut site. The PCR products were digested with their respective restriction enzymes and then ligated into the expression vector pProEX htc (Life Technologies), which includes an N-terminal His_6-tag rTEV cleavage site and an ampicillin-resistance gene. The resultant plasmids, pNDsbC and pNDsbG, were transformed into *E. coli* (DH5α) by electroporation and colonies with the plasmids were selected using ampicillin. Each construct was confirmed by DNA sequencing.

2.2. Protein expression and purification

The plasmids pNDsbC and pNDsbG were transformed into the *E. coli* BL21 (DE3) expression strain. For large-scale expression, Luria–Bertani broth (containing 100 µg ml^{-1} ampicillin) was inoculated with a 1:100 ratio of an overnight preculture. When the cell culture reached an OD_{600} of 0.6–0.8, expression of recombinant proteins was induced with 0.5 m*M* isopropyl β-D-thiogalactopyranoside (IPTG) at 310 K overnight. Cell pellets were lysed using a cell disrupter (Constant System) in a lysis buffer containing 50 m*M* 4-(2-hydroxyethyl)-1-piperazine-1-ethanesulfonic acid (HEPES) pH 7.5

and 300 m*M* NaCl. The His_6-tagged protein was purified using an Ni^{2+}-charged 5 ml HiTrap chelating column (Amersham Biosciences) equilibrated in the lysis buffer and eluted with a stepwise gradient of imidazole (up to 300 m*M*). The His_6 tag was cleaved by recombinant tobacco-etch virus (rTEV) protease and recombinant protein was isolated by a second application of the HiTrap column. Further purification was carried out by size-exclusion chromatography with a Superdex 75 10/30 column (Amersham Biosciences) in a buffer containing 25 m*M* HEPES pH 7.5, 150 m*M* NaCl. The purity of the protein was checked by SDS–PAGE.

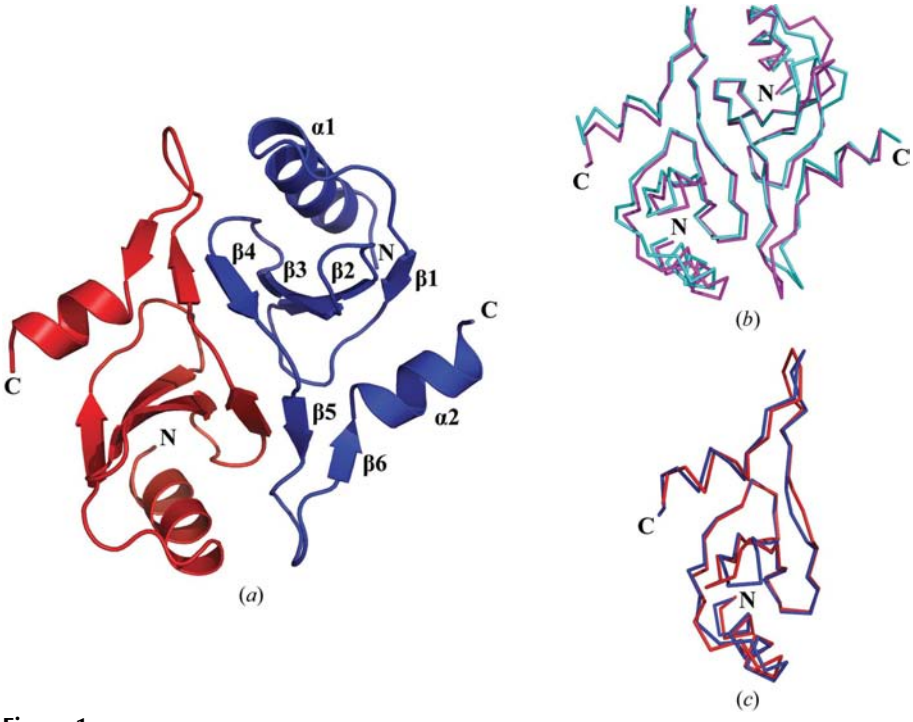

Figure 1
(*a*) Structure of the NDsbC homodimer. (*b*) Superposition of the C^{α} traces of the NDsbC dimer (magenta) and of the dimer formed by the N-terminal 71 residues of native DsbC (cyan). (*c*) Superposition of the C^{α} traces of the NDsbC monomers (molecule *A*, red; molecule *B*, blue).

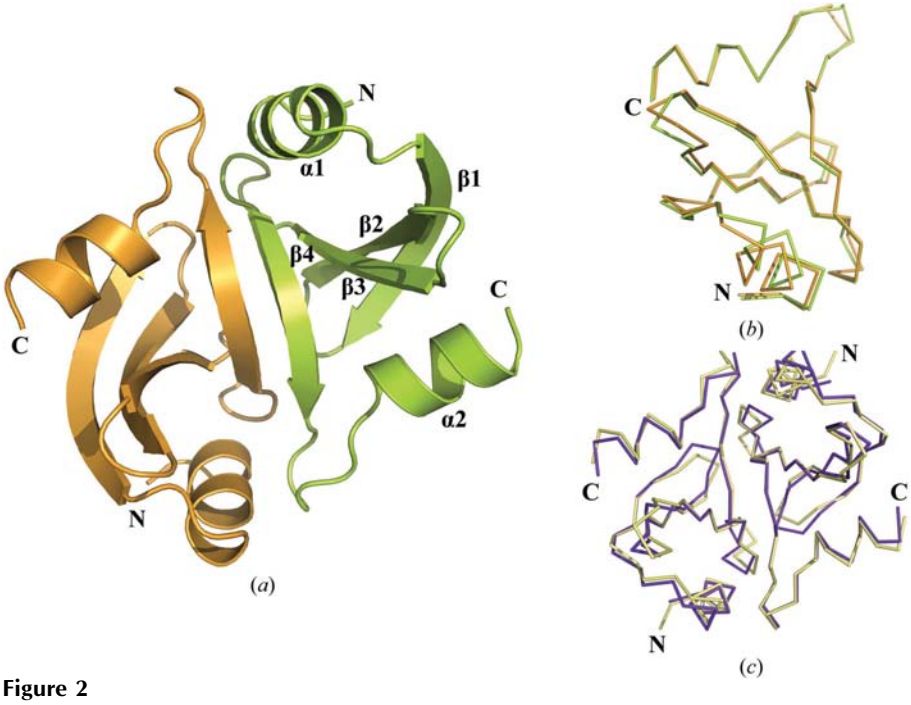

Figure 2
(*a*) Structure of the NDsbG homodimer. (*b*) Superposition of the C^{α} traces of the NDsbG monomers (molecule *A*, green; molecule *B*, orange). (*c*) Superposition of the C^{α} traces of the NDsbG dimer (purple) and the dimer formed by native DsbG residues (yellow).

2.3. Crystallization

The purified NDsbC protein was concentrated to between 3 and 6 mg ml^{-1}. Initial crystallization conditions were established using the sitting-drop vapour-diffusion method with 100 + 100 nl drops delivered by a Cartesian Honeybee robotic device (Genomic Solutions). Fine screens were carried out manually using 96-well sitting-drop plates with 1 µl protein solution mixed with 1 µl reservoir solution containing 2.0 *M* Li_2SO_4, 0.1 *M* $MgSO_4$ and 5% 2-propanol pH 4.5. NDsbC crystals appeared overnight and grew as hexagonal plates. Prior to data collection, all crystals were briefly immersed in cryoprotectant (a 4:1 mixture of reservoir and glycerol) and were then frozen in liquid nitrogen.

The initial crystallization trials of NDsbG were performed as for NDsbC, except that the protein concentration was in the range 3–4 mg ml^{-1}. Fine screens were then performed manually as before using the sitting-drop vapour-diffusion method, varying the cadmium chloride concentration in the range 0–0.3 *M* and the MPD concentration in the range 20–45%. Clusters of rod-shaped NDsbG crystals appeared overnight. The crystal used for structure determination was prepared using a reservoir solution containing 0.2 *M* cadmium chloride and 33%(*v*/*v*) MPD. NDsbG crystals were frozen in liquid nitrogen without additional cryoprotectant.

2.4. Data collection and processing

NDsbC X-ray diffraction data were collected to a maximum resolution of 2.0 Å at beamline BL 9-1 at the Stanford Synchrotron Radiation Laboratory (SSRL) using an ADSC Q315 CCD detector. The crystal-to-detector

distance was 350 mm and images were collected with a 0.5° oscillation angle. The images were processed and the data were scaled with the *HKL* software package (Otwinowski & Minor, 1997).

Diffraction data for NDsbG were collected at the Swiss Light Source (SLS) using beamline PX1 in micro-focus mode with a MAR165 CCD detector at a crystal-to-detector distance of 120 mm and an oscillation angle of 1°. To minimize radiation damage from the intense microbeam, data were collected in 40° segments from different portions of the crystal. Prior to data collection, the crystals were 'flash-annealed' (Yeh & Hol, 1998) by blocking the cryostream cooling flow briefly. All data were processed and scaled with *MOSFLM* (Leslie, 1992) and *SCALA* (Kabsch, 1988; Collaborative Computational Project, Number 4, 1994).

2.5. Structure determination

The structures of both NDsbC and NDsbG were solved by molecular replacement using search models consisting of residues 1–71 of the DsbC monomer (PDB code 1eej) and of residues 1–71 of the full-length DsbG monomer (PDB code 1v58), respectively. Molecular replacement was performed using *MOLREP* (Vagin & Teplyakov, 1997) for NDsbC and *Phaser* (Storoni *et al.*, 2004) for NDsbG. The program *Coot* (Emsley & Cowtan, 2004) was used for fitting and viewing of electron-density maps for both structures.

The NDsbC structure was refined using *CNS* (Brünger *et al.*, 1998) with iterative cycles of simulated annealing, conjugate-gradient minimization and *B*-factor refinement in the resolution range 44.8–2.0 Å. The final refinement steps were carried out using the TLS refinement option in *REFMAC* (Murshudov *et al.*, 1997), treating the monomer as one entity. Alternative space groups and possible twinning operators were checked using *XTRIAGE* (Zwart *et al.*, 2006). The final model has an *R* factor of 0.227 ($R_{\rm free}$ = 0.251). The structure has good stereochemistry, with 94.2% of residues in the most favoured region of the Ramachandran plot and 5.8% of residues in the additionally allowed region.

The NDsbG structure was refined in *REFMAC* (Murshudov *et al.*, 1997). The final structure has good stereochemistry and was refined to 1.9 Å resolution with an *R* factor of 0.196 ($R_{\rm free}$ = 0.237). The structure of NDsbG has 94.2% and 5.8% of residues in the most favoured and additionally allowed regions of the Ramachandran plot, respectively. The complete refinement statistics for both models are given in Table 1.

All figures were generated using *PyMOL* (DeLano, 2002). The buried surface area was calculated using *GRASP* (Nicholls, 1993).

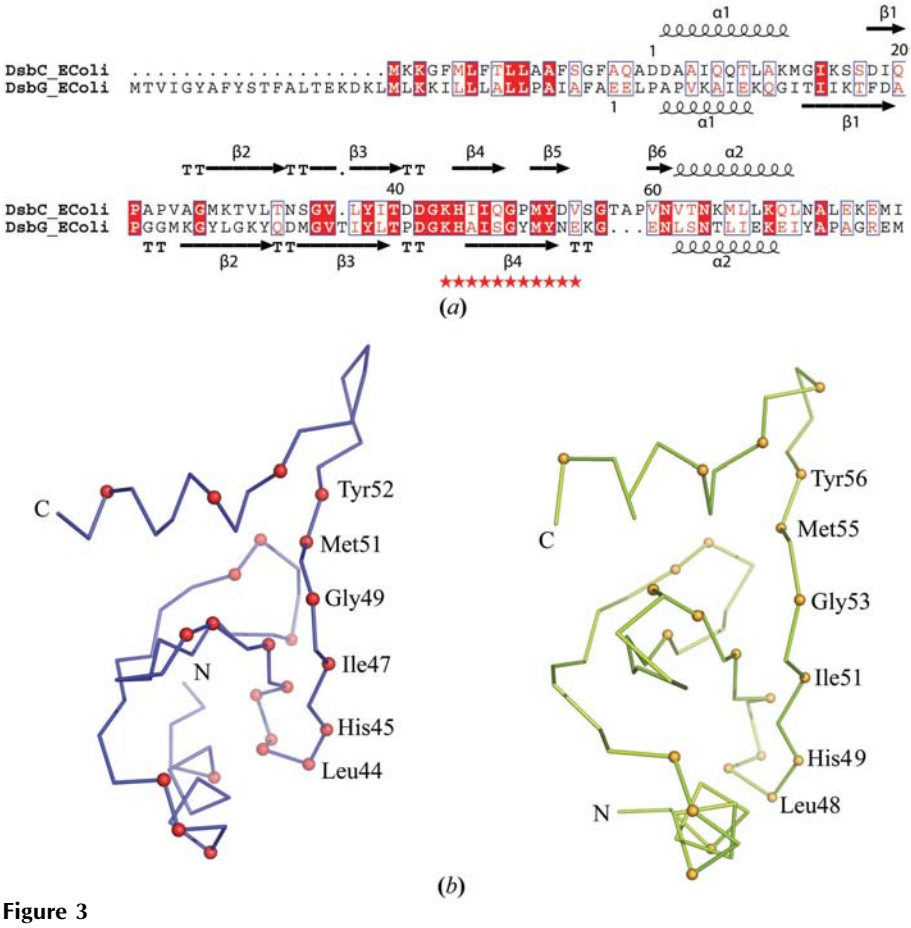

Figure 3
(*a*) Sequence alignment of the 90 N-terminal residues of *E. coli* DsbC and DsbG. Secondary-structure elements are based on the NDsbC (top) and NDsbG (bottom) structures and those residues contributing to the dimer interface are indicated by red stars. Identical residues are shown in red boxes. (*b*) The location of identical amino acids (red spheres in NDsbC; orange spheres in NDsbG) in the C^{α} traces of monomers of NDsbC (blue) and NDsbG (green). The identical residues involved in the dimer interface are labelled. The sequence alignment was performed using *ESPript* v.2.2.

3. Results and discussion

3.1. The DsbC dimerization domain NDsbC

The final NDsbC model (PDB code 2iyj) contains two monomers (*A* and *B*) in the asymmetric unit. These display approximate twofold symmetry and form the biological dimer. The approximate solvent content of the crystal is 31%. All main-chain atoms of NDsbC are included in the model, with the exception of residue 71 at the C-terminus of monomer *A*. Some side chains (Lys15 and Ser16 in molecule *A* and Lys11, Met12, Lys15 and Lys44 in molecule *B*) were not able to be modelled owing to weak electron density. One sulfate ion was identified in the asymmetric unit, interacting with the side chains of Asp41 (*A*), Lys28 (*A*), and a water molecule.

The domain is an approximately symmetrical structure. It consists of two six-stranded antiparallel β-sheets in which strands 1–4 are contributed by one monomer and strands 5 and 6 are contributed by the other monomer. Each monomer comprises an N-terminal α-helix (α1) followed by a four-stranded antiparallel β-sheet (β1–4), a β-hairpin (β5–6) and a short α-helix (α2) (Fig. 1*a*). The overall structure of NDsbC is very similar to that of the N-terminal dimerization domain of oxidized *E. coli* DsbC (PDB code 1eej), except for the flexible loop regions (residues 14–19 between α1 and β1, residues 31–36 between β2 and β3 and residues 54–60 between β6 and α2; Fig. 1*b*).

The two molecules in the asymmetric unit are similar and *A* superposes on *B* with an r.m.s. difference in C^{α} positions of 1.0 Å over residues 1–70 from each molecule (Fig. 1*c*). Differences occur between the two molecules at the C/N-terminal residues, the flexible loops (residues 14–18, 32–35 and 54–56) and the central region of the dimer interface (residues 48–50). In the latter region, the main-chain O atoms of Gln48 are oriented in opposite directions and there is a difference in the C^{α} position of Gly49 of 1.7 Å. This asymmetry between the *A* and *B* molecules at the dimer interface is also seen in the full-length DsbC structure (PDB code 1eej) and DsbC C101S (PDB code 1jzo).

3.2. The DsbG dimerization domain NDsbG

The final model of NDsbG (PDB code 2iy2) also contains two molecules (*A* and *B*) in the asymmetric unit, in which 134 of 148 residues are visible. The solvent content of the crystal is approximately 39.4%. No electron density was found for the two extra vector-derived residues Met1 and Glu2 or for the C-terminal Cys72 in both molecules. The loop between β2 and β3 was difficult to model because of poor electron density and residues 35 and 36 were not modelled in molecule *B*. Some side chains were also not modelled (Lys28, Met37, Glu58 and Gln69 in molecule *A*, and Lys12 and Lys33 in molecule *B*). Four metal ions were identified in the asymmetric unit, coordinated to water molecules and the side chains of residues Asp46 and a symmetry-related Asp22 or His49. These ions were modelled as cadmium (the crystallization buffer contained 0.2 *M* cadmium chloride) and stabilize the crystal structure by cross-linking adjacent molecules.

In the structure of full-length DsbG (PDB code 1v58), the biological dimer is a result of crystal symmetry and for that reason shows perfect symmetry. In contrast, the crystals of the truncated structure contain the biological dimer in the asymmetric unit, with noncrystallographic twofold symmetry relating the two monomers. Each monomer consists of an α-helix (α1) followed by four β-strands (β1–4) and a truncated α-helix (α2) (Fig. 2*a*). Despite the lack of crystallographic symmetry, the two molecules in the asymmetric unit are very similar (r.m.s. difference in C^{α} positions ∼0.7; Fig. 2*b*). Apart from the flexible loops (residues 23–28 between β1 and β2, residues 32–39 between β2 and β3, residues 44–48 between β3 and β4, and residues 57–61 between β4 and α2), the structure of the NDsbG dimer is very similar to the corresponding dimer formed by the N-terminal domain of full-length DsbG (PDB code 1v58) after generating this dimer by symmetry (Fig. 2*c*)

3.3. Comparison of the dimer interfaces of NDsbC and NDsbG

Both the NDsbC and NDsbG dimer interfaces contain hydrophobic interactions and hydrogen bonds. The total buried surface area is approximately 1200 $Å^2$ (600 $Å^2$ for each monomer) or ∼15% of the monomer surface for both NDsbC and NDsbG. The dimer interface of NDsbC is composed of residues 44–54 from each monomer located on strands β4 and β5. Residue Gly49, located at the centre of the dimer interface, is highly conserved (McCarthy *et al.*, 2000) and is essential for dimerization (Bader *et al.*, 2001). The NDsbG dimer interface consists of residues 48–58 from each monomer. These residues also have a high degree of conservation (Heras *et al.*, 2004). At the centre of the NDsbG/DsbG dimer interface, Gly53 is located at the equivalent position to

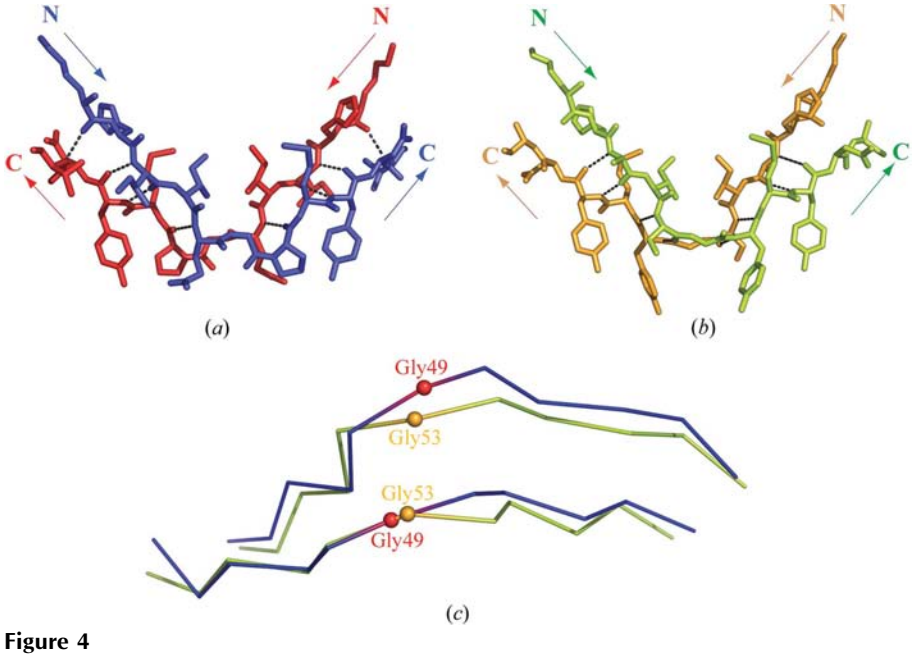

Figure 4
(*a*) and (*b*) Diagrams presenting the hydrogen-bond interactions in the dimer interface of the NDsbC dimer (*a*) and the NDsbG dimer (*b*). Monomers *A* and *B* in the NDsbC dimer are shown in red and blue, respectively, and monomers *A* and *B* in the NDsbG dimer are shown in green and orange, respectively. The orientations from the N-terminus toward the C-terminus are indicated by arrows. Hydrogen-bond interactions are shown as dashed lines. (*c*) Superposition of the C^{α} traces of the NDsbC (blue) and NDsbG dimer interfaces (green). The central Gly residues are represented by red spheres in NDsbC and by orange spheres in NDsbG.

Gly49 of DsbC. Although there have been no published investigations on the significance of Gly53 in DsbG, its strictly conserved nature and position in the dimer interface would suggest that it plays a similar role.

The NDsbC and NDsbG dimer interfaces show strong similarities in amino-acid sequence and structural conformation. NDsbC and NDsbG show 32% overall sequence identity at the protein level (Fig. 3*a*). Identical residues between NDsbC and NDsbG are particularly found in the dimer interface and in the loop prior to the dimer interface (Fig. 3*b*). These residues are significant in maintaining and stabilizing the overall structural conformations. Both dimer interfaces are arranged as antiparallel β-strands and have a V-shaped conformation when viewed along the dimer interface normal to the local twofold symmetry axis (Figs. 4*a* and 4*b*). In NDsbC, *cis*-Pro50 introduces a $\sim$90° bend to the main chain, resulting in the two halves of the dimer drawing closer to each other. A similar geometry for the main chain is found in the NDsbG dimer interface, with bending contributed by Tyr54 and Ser52. When the NDsbC interface is superimposed onto that of NDsbG, the main-chain C^{α}-trace conformations between the two are highly similar. However, the distance between the C^{α} positions of the NDsbC Gly49 pair is 6.1 Å, whereas the corresponding distance for the Gly53 pair in NDsbG has a separation of 4.2 Å, making the central region of the interface 50% wider in DsbC (Fig. 4*c*).

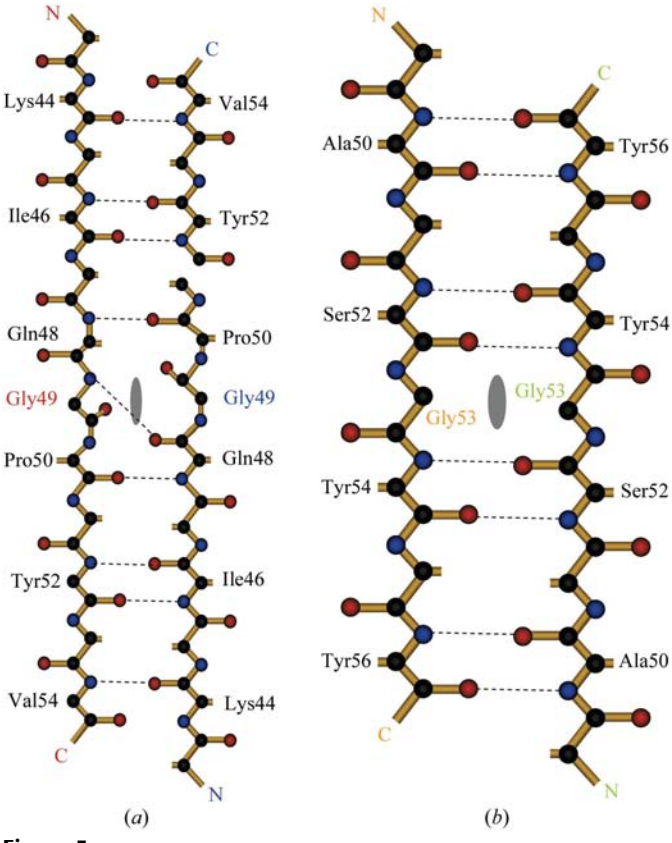

Figure 5
(*a*) Diagram representing the dimeric antiparallel β-sheet interface of NDsbC. The central hydrogen bond (formed between Gly49 on molecule *A* and Asn48*A* on molecule *B*) crosses the twofold axis (grey filled oval) perpendicular to the plane of the page. The N- and C-termini are labelled in red for molecule *A* and in blue for molecule *B*. (*b*) Diagram representing the dimeric antiparallel β-sheet in the dimer interface of NDsbG. The local twofold axis (grey filled oval) is perpendicular to the plane of the page, between a pair of Gly residues that are not hydrogen bonded to each other. The N- and C-termini are labelled in orange for molecule *A* and in green for molecule *B*. Hydrogen bonds are represented as dashed lines.

The NDsbC dimer interface involves four equivalent pairs of main-chain hydrogen bonds: one pair between Lys44 and Val54, two pairs between Ile46 and Pro50 and one pair between Gln48 and Pro50 (Fig. 5*a*). One hydrogen bond is observed between the backbone amide of Gly49 (*A*) and the carbonyl O atom of Glu48 (*B*). However, this corresponding bond is not found between Gly49 (*B*) and Glu48 (*A*). This asymmetry in hydrogen bonding is also seen in the dimer interface of full-length DsbC (PDB code 1eej) and DsbC C101S (PDB code 1jzo).

The pattern of hydrogen bonding in the NDsbG dimer interface is distinct from that in NDsbC. In NDsbG, the twofold axis of the biological dimer is at the centre of the pair of Gly53 residues, with no hydrogen bonds between these residues (Fig. 5*b*). Brown (2006) describes this type of symmetry in the interface as 'NHB' (non-hydrogen bonded). Two pairs of hydrogen bonds are formed between the main-chain atoms of Ala50/Tyr56 and Ser52/Trp54 (eight in total, including equivalent pairs across the symmetry axis). These observations are consistent with the symmetry-generated biological dimer of full-length DsbG.

The distinct hydrogen-bonding patterns between the dimer interfaces of DsbC and DsbG may result from different environments surrounding the interface. Several water molecules were observed in both full-length DsbC and NDsbC and both Gln48 residues in the DsbC dimer interface have very flexible solvent-exposed side chains with high *B* factors. Furthermore, the backbone carbonyl group of Gln48 in molecule *B* is oriented toward the dimer interface, whereas in molecule *A* it points away from the interface. Fewer water molecules were found in the DsbG/NDsbG dimer interfaces and the Ser52 residues corresponding to DsbC Gln48 are both oriented with the carbonyl groups pointing inwards towards the dimer interface. Although these serine residues also have solvent-exposed side chains that bind water molecules, the *B* factors for these atoms are lower than the equivalent residues in DsbC, indicating less flexibility.

3.4. A potential linker using NDsbC or NDsbG

The N-terminal dimerization domain of DsbC has been used as part of chimeric constructs to study DsbC disulfide-bond isomerase and chaperone activity *in vitro* and *in vivo* (Segatori *et al.*, 2004; Zhao *et al.*, 2003). Briefly, DsbC chimeras were constructed by substituting the catalytic domain with thioredoxin (TrxA) or DsbA. These chimeras were found to be dimers by HPLC analysis. This dimeric feature of NDsbC hybrids is consistent with our observations of the nature of dimerization of the DsbC N-terminal domain. The DsbG dimerization domain has not been as widely investigated. However, since the DsbC and DsbG dimerization domains

show similarity at the three-dimensional structure level, we presume that if monomeric molecules were generated in which the C-terminal thioredoxin fold domain of DsbG was replaced, such chimeras would also self-assemble and form dimers. The independent folding nature and stability of the DsbC/G dimerization domains have the potential to be developed into useful linkers for practical applications.

We thank Dr Tom Caradoc-Davies, Dr David Goldstone and Richard Bunker for assistance in resolving the atomic structure. We are grateful to A. Lebedev for providing valuable advice for NDsbC data processing, Elaine Chiu for help with cloning and E. Baker for proofreading. The plasmids encoding full-length *E. coli* DsbC and DsbG were kind gifts from J. Bardwell. This work was supported by the New Economy Research Fund (NERF) and S-MY is a recipient of the Top Achiever Doctoral Scholarship from the New Zealand Government.

References

Andersen, C. L., Matthey-Dupraz, A., Missiakas, D. & Raina, S. (1997). *Mol. Microbiol.* **26**, 121–132.
Bader, M. W., Hiniker, A., Regeimbal, J., Goldstone, D., Haebel, P. W., Riemer, J., Metcalf, P. & Bardwell, J. C. (2001). *EMBO J.* **20**, 1555–1562.
Banaszak, K., Mechin, I., Frost, G. & Rypniewski, W. (2004). *Acta Cryst.* D**60**, 1747–1752.
Bessette, P., Cotto, J., Gilbert, H. & Georgiou, G. (1999). *J. Biol. Chem.* **274**, 7784–7792.
Brown, J. (2006). *Protein Sci.* **15**, 1–13.
Brünger, A. T., Adams, P. D., Clore, G. M., DeLano, W. L., Gros, P., Grosse-Kunstleve, R. W., Jiang, J.-S., Kuszewski, J., Nilges, M., Pannu, N. S., Read, R. J., Rice, L. M., Simonson, T. & Warren, G. L. (1998). *Acta Cryst.* D**54**, 905–921.
Chen, J., Song, J. L., Zhang, S., Wang, Y., Cui, D. F. & Wang, C. C. (1999). *J. Biol. Chem.* **274**, 19601–19605.
Collaborative Computational Project, Number 4 (1994). *Acta Cryst.* D**50**, 760–763.
DeLano, W. L. (2002). *The PyMOL Molecular Graphics System.* http://www.pymol.org.
Emsley, P. & Cowtan, K. (2004). *Acta Cryst.* D**60**, 2126–2132.
Goldstone, D., Haebel, P. W., Katzen, F., Bader, M. W., Bardwell, J. C., Beckwith, J. & Metcalf, P. (2001). *Proc. Natl Acad. Sci. USA*, **98**, 9551–9556.
Haebel, P. W., Goldstone, D., Katzen, F., Beckwith, J. & Metcalf, P. (2002). *EMBO J.* **21**, 4774–4784.
Heras, B., Edeling, M. A., Schirra, H. J., Raina, S. & Martin, J. L. (2004). *Proc. Natl Acad. Sci. USA*, **101**, 8876–8881.
Kabsch, W. (1988). *J. Appl. Cryst.* **21**, 916–924.
Kadokura, H., Katzen, F. & Beckwith, J. (2003). *Annu. Rev. Biochem.* **72**, 111–135.
Leslie, A. G. W. (1992). *Jnt CCP4/ESF–EACBM Newsl. Protein Crystallogr.* **26**.
McCarthy, A. A., Haebel, P. W., Torronen, A., Rybin, V., Baker, E. N. & Metcalf, P. (2000). *Nature Struct. Biol.* **7**, 196–199.
Murshudov, G. N., Vagin, A. A. & Dodson, E. J. (1997). *Acta Cryst.* D**53**, 240–255.
Nicholls, A. J. (1993). *Biophys. J.* **64**, A116.
Otwinowski, Z. & Minor, W. (1997). *Methods Enzymol.* **276**, 307–326.
Segatori, L., Paukstelis, P. J., Gilbert, H. F. & Georgiou, G. (2004). *Proc. Natl Acad. Sci. USA*, **101**, 10018–10023.
Shao, F., Bader, M., Jakob, U. & Bardwell, J. (2000). *J. Biol. Chem.* **275**, 13349–13352.
Storoni, L. C., McCoy, A. J. & Read, R. J. (2004). *Acta Cryst.* D**60**, 432–438.
Vagin, A. & Teplyakov, A. (1997). *J. Appl. Cryst.* **30**, 1022–1025.
Yeh, J. I. & Hol, W. G. J. (1998). *Acta Cryst.* D**54**, 479–480.
Zwart, P., Grosse-Kunstleve, R. & Adams, P. (2006). *CCP4 Newslett.* **8**, Summer.
Zhao, Z., Peng, Y., Hao, S. F., Zeng, Z. H. & Wang, C. C. (2003). *J. Biol. Chem.* **278**, 43292–43298.